34. Ballhausen, C. J.; Gray, H. B. *Molecular Orbital Theory*; W. A. Benjamin Inc.: New York, 1964; p 120.
35. McGlynn, S. P.; Vanquickenborne, L. G.; KIinoshita, M.; Caroll, D. G.*Introduction to Applied Quantum Chemistry*; Hott, Rinehart and Winston Inc.: New York, 1972; p 423.
36. Wells, A. F. *Structural Inorganic Chemistry*; Clarendon Press.: Oxford, 1984; p 498.

Spectroscopic Properties and Ligand Field Analysis of Tris[(±)-*trans*-1,2-cyclohexanediamine]chromium(III) Chloride[1]

Jong-Ha Choi

Department of Chemistry, Andong National University, Andong 760-749
Received September 3, 1993

The low temperature luminescence and excitation, room-temperature UV-visible and infrared spectra of $[Cr(\pm)chxn_3]Cl_3$ (chxn=*trans*-1,2-cyclohexanediamine) have been measured. It is found that the zero-phonon line in the excitation spectrum splits into two components by 47 cm^{-1}. The eight electronic transitions due to spin-allowed and spin-forbidden are assigned. As expected, nitrogen atoms of chxn ligand have strong σ-donor properties toward chromium(III). The positions and splittings of sharp-line transitions are analyzed as a function of the Cartesian bite (α) and twist (β) angles to predict the metal-ligand geometry.

Introduction

Sharp-line electronic spectroscopy has provided a powerful tool for extracting geometric informations.[2] The sharp-line electronic transitions are very sensitive to the exact bond angles around the metal. Thus it is possible to obtain a structural information from sharp-line electronic spectrum quickly without a full X-ray structure determination.

Luminescence, absorption and excitation spectroscopic studies of chromium(III) complexes began with hexacoordinated nitrogen complexes, because their intensities tend to be quite strong. A number of such complexes have already been investigated.[3] The spectroscopic properties of CrN_6 complexes are very similar, although the photochemical quantum yields vary considerably. Wasgestian and Gowin have reported photosubstitution quantum yields of chromium(III) complexes with CrN_6 skeletons in acid solution.[4]

When a cyclohexane ring is fused with a five-membered chelate ring, the chelate ring is not able to exhibit the puckering motion. Hence, it was possible to separate and characterize eight possible isomers of $[Cr(chxn)_3]^+$ ion.[5] The X-ray crystal structure of *lel*$_3$-$[Cr(chxn)_3](NO_3)_3 \cdot 3H_2O$ has been studied.[6] The electrostatic and hydrophobic interactions in the ion associations between the $[Cr(chxn)_3]^+$ ion and the sulfonate anions have been investigated.[7] The absorption and circular dichroism spectra in the spin-forbidden transitions have also been reported.[8]

We have measured the 77 K luminescence and 12 K excitation, and room-temperature UV-visible and infrared spectra of $[Cr(\pm)chxn_3]Cl_3$. In this paper we describe its spectroscopic and ligand field properties. The relationship between the metal-ligand geometry and the sharp-line electronic transitions is discussed.

Experimental Section

Synthesis. All chemicals were reagent grade quality and used without further purification. Tris[(±)-*trans*-1,2-cyclohexanediamine]chromium(III) chloride was prepared according to Pederson's method[9] by use of racemic *trans*-1,2-cyclohexanediamine. The compound was recrystallized three times for spectroscopic measurements.

Measurements and Computations. The room-temperature absorption spectrum in aqueous solution was recorded with a Hewlett-Packard Model 8451A diode array spectrophotometer. The far-infrared spectrum was recorded with a Bruker 113 V instrument on a microcrystalline sample pressed in to a polyethylene pellet. These measurements were done at room-temperature by Dr T. Schönherr at the University of Düsseldorf. The mid-infrared spectrum was recorded with a Mattson 2020 Galaxy FT-IR spectrometer on a KBr pellet. The luminescence spectrum was measured at 77 K on a Spex Fluorolog-2 spectrofluorometer as previously described.[3c]

The excitation spectrum of $[Cr(\pm)chxn_3]Cl_3$ at 12 K was measured by monitoring the luminescence intensity of the vibronic sideband at 709 nm. The light from an EG & G PAR Dyescan nitrogen laser-pumped dye laser was focused on a microcrystalline sample mounted with conductive grease on the cold head of an Air Products Displex CSA-202E cryostat. The emitted light was dispersed by a Spex Double 220 mm monochromator with 0.5 mm slits. The output from a cooled Hamamatsu R928 photomultiplier was passed to an SRS boxcar integrator, triggered by a fraction of the laser pulse passed to a fast photodiode. The excitation wavelength was calibrated by using four neon optogalvanic resonance points. The excitation spectrum was corrected for the laser

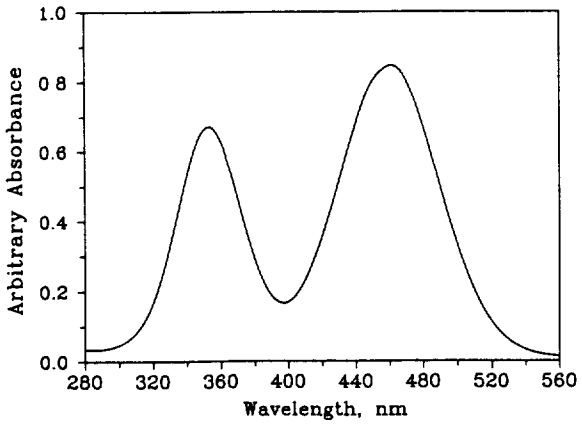

Figure 1. Electronic absorption spectrum of $[Cr(\pm)chxn_3]^{3+}$ in aqueous solution at room temperature.

intensity.

All optimizations and calculations for the ligand field analysis were performed on an IBM mainframe computer. Some smaller computations and data manipulations were done on IBM compatible 486 DX_2-66 microcomputer with an 8 MB main memory.

Results and Discussion

Absorption Spectrum. The electronic absorption spectrum of $[Cr(\pm)chxn_3]Cl_3$ may be interpreted on the basis of a $[CrN_6]^{3+}$ ion in near octahedral environment as follows. Hexacoordinated chromium(III) complexes exhibit three spin-allowed transitions from the ground state $^4A_{2g}(F)$ to $^4T_{2g}$ (ν_1), $^4T_{1g}(F)$ (ν_2) and $^4T_{1g}(P)$ (ν_3) in O_h notation.[10] The third band, ν_3 usually occurs above 30,000 cm^{-1} and would be obscured by ligand or charge-transfer absorption in this region.[11] The visible absorption spectrum of $[Cr(\pm)chxn_3]Cl_3$ in aqueous solution is represented in Figure 1.

It exhibits two bands, one at 21,752 cm^{-1}(ν_1) and the other at 28,303 cm^{-1}(ν_2) corresponding to the $^4A_{2g}\rightarrow{}^4T_{2g}$ and $^4A_{2g}\rightarrow{}^4T_{1g}(O_h)$ transitions, respectively. These bands resemble closely those observed for other octahedral $[CrN_6]^{3+}$ complexes. Within conventional ligand field theory, the energy of the first spin-allowed transition, $^4A_{2g}\rightarrow{}^4T_{2g}(\nu_1)$ gives the value of the ligand field splitting parameter, $10Dq$ directly. The value of the ratio, ν_2/ν_1 is 1.301. We find that this value corresponds to $Dq/B=3.563$, $\nu_3/B=75.542$, $\nu_3/\nu_1=2.121$ and $\nu_3/\nu_2=1.631$ from the Table[11] of transition energy ratios for A_2 ground term in the cubic complexes. The angular overlap model parameter, e_σ is readily obtained from the relation, $10Dq=3e_\sigma-4e_\pi$ because π-bonding for the amine nitrogen is approximately zero. However, it is noteworthy that the π-bonding ability of nitrogen with sp^2 hybridization cannot be neglected. Peptide nitrogen, for example, is a weak π-donor.[12] The ligand parameters deduced based on the broad band spectrum for $[Cr(chxn)_3]^{3+}$ are $Dq=2{,}175$ cm^{-1}, $B=611$ cm^{-1} and $e_{\sigma N}=7{,}251$ cm^{-1}. These parameters were used as input data for a complete ligand field analysis, including the sharp-line electronic transitions. The transition to the $^4T_{1g}(P)$ state is also predicted to lie at about 46,150 cm^{-1}. The third band corresponding to this transition was not detectable in the UV-visible spectrum.

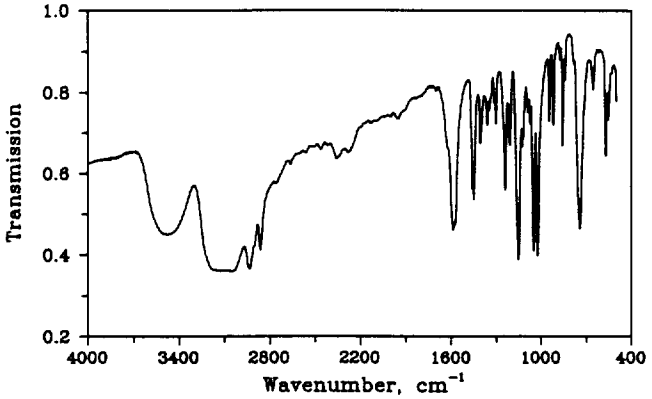

Figure 2a. Mid-infrared spectrum of $[Cr(\pm)chxn_3]Cl_3$ at room temperature.

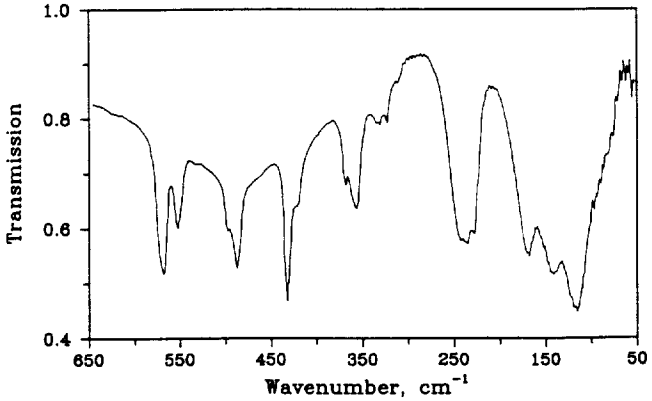

Figure 2b. Far-infrared spectrum of $[Cr(\pm)chxn_3]Cl_3$ at room temperature.

Infrared Spectrum. Figures 2a and 2b present the mid- and far-infrared spectra of $[Cr(\pm)chxn_3]Cl_3$ recorded at room-temperature.

A broad absorption peak at 3,480 cm^{-1} can readily be assigned to the O-H stretching of the water of crystallization. The strong bands in the 3,200-3,100 cm^{-1} and 3,000-2,800 cm^{-1} regions are due to the symmetric and antisymmetric N-H and C-H stretching modes, respectively. The absorption bands at 1,587, 1,453 and 1,405 cm^{-1} can be assigned to the CH_2 and NH_2 bending modes. The absorption bands in the region of 2,200-1,400 cm^{-1} are due to the wagging modes of NH_2 and CH_2. The strong peaks at 859 and 746 cm^{-1} are primarily involved in the NH_2 and CH_2 rocking modes, respectively. The Cr-N stretching bands were detected in range 490-420 cm^{-1}. In the spectrum of $[Cr(NH_3)_6]Cl_3$, there is a single peak at 469 cm^{-1}.[13] A number of absorption bands in the range 370-110 cm^{-1} arise from ring deformations and lattice vibrations.

Luminescence Spectrum. The 465 nm excited 77 K luminescence spectrum of $[Cr(\pm)chxn_3]Cl_3$ is shown in Figure 3. The band positions relative to the lowest zero-phonon line, with corresponding infrared frequencies, are listed in Table 1. The luminescence spectrum was independent of the exciting wavelength within the first spin-allowed transition region.

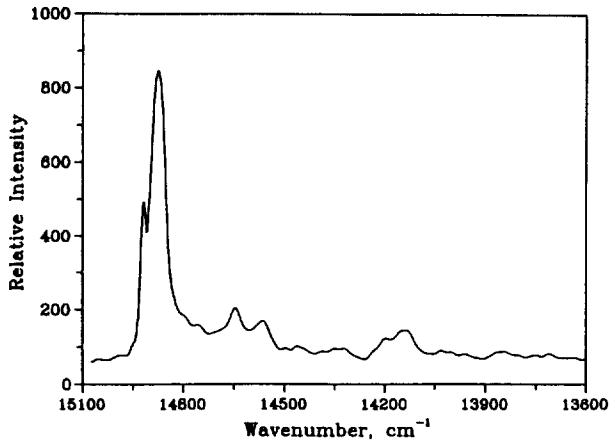

Figure 3. The 77 K luminescence spectrum of $[Cr(\pm)chxn_3]Cl_3$ (λ_{ex}=465 nm).

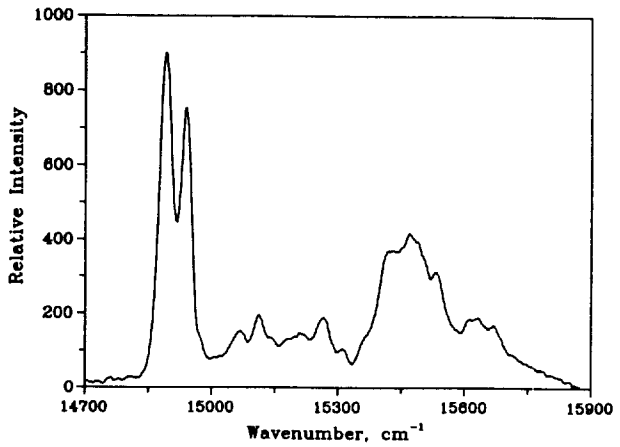

Figure 4. The 12 K excitation spectrum of $[Cr(\pm)chxn_3]Cl_3$ (λ_{em}=709 nm).

Table 1. Vibrational Frequencies from the 77 K Luminescence and 298 K Infrared Spectra for $[Cr(\pm)chxn_3]Cl_3$[a]

Luminescence[b]	Infrared	Assignment
−44 vs		R_2
0 vs		R_1
119 w	112 m, 121 m	Lattice and δ(N-Cr-N)
160 w	143 m, 171 s	
231 s	228 m, 238 s, 244 m	
310 m	309 vw, 323 w	
382 vw	359 s, 370 m	
414 w	423 sh	ν(Cr-N)
443 vw	442 vs	
464 w		
488 w	490 vs, 500 m	
536 w	555 s	ν(Cr-N)+Ring def.
583 sh	573 s	
676 m	658 m	
741 s	746 vs	ρ(CH_2)
779 sh		
844 w	859 m	ρ(NH_2)
879 w		
922 w	920 mw	
975 vw	948 w	
1038 w	1022 vs	
1074 vw	1052 vs	
1111 vw	1123 vw	
1165 w	1153 vs	

[a] Data in cm^{-1}. [b] Measured from zero-phonon line at 14879 cm^{-1}.

The very strong peak at 14,879 cm^{-1} can be assigned to the zero-phonon line, R_1 because a corresponding strong peak is found at 14,881 cm^{-1} in the excitation spectrum. A well defined hot band at 14,923 cm^{-1} which may be assigned to the second component of the $^2E_g \rightarrow {}^4A_{2g}$ transition. The vibronic intervals occurring in the spectrum consist of several modes can be presumed to involve primarily ring torsion and angle-bending modes with frequencies below 382 cm^{-1}. The band at 463 cm^{-1} can be assigned as a Cr-N stretching mode. The weak bands at 414 and 443 cm^{-1} in the luminescence spectrum have relatively strong counterparts in the infrared spectrum, and can also be assigned as Cr-N stretching modes.

Excitation Spectrum. The 12 K excitation spectrum is shown in Figure 4. The peak positions and their assignments are tabulated in Table 2. The calculated frequecies in parentheses was obtained by using the vibrational modes ν_1-ν_7 listed in Table 2.

Two strong peaks at 14,881 and 14,928 cm^{-1} in the excitation spectrum coincide with the luminescence spectrum are assigned to the two components (R_1 and R_2) of the $^4A_{2g} \rightarrow {}^2E_g$ transition. The lowest-energy zero-phonon line coincides within 2 cm^{-1} with the emission origin. The observed 47 cm^{-1} splitting is large, compared with the 18 cm^{-1} of $2Cr(en)_3Cl_3 \cdot 6H_2O \cdot KCl$.[13] The three components of the $^4A_{2g} \rightarrow {}^2T_{1g}$ electronic origin (T_1, T_2 and T_3) can be found with strong intensities 565, 632 and 713 cm^{-1} from the lowest electronic line. Vibronic bands based on these origins also have similar frequencies and intensity patterns to those of the ^2E_g components.

Since no electronic origin was found in the region 300-400 cm^{-1} above the $^4A_{2g} \leftrightarrow {}^2E_g$ transition, the activation energy of that magnitude observed for line broadening in solution cannot be ascribed to thermal population of a low-lying $^2T_{1g}$ component. However, population of a vibronic level of either ^2E_g component can rationalize the experimental observations.

The higher energy $^4A_{2g} \rightarrow {}^2T_{2g}$ band was found at 22,352 cm^{-1} from the second derivative of the solution absorption spectrum of $[Cr(chxn)_3]^{3+}$, shown with label (b) in Figure 5, but it could not be resolved into the separate components.

Ligand Field Analysis. The ligand field potential was constructed with only the six coordinated nitrogen atoms. Angular overlap parameter provide more chemical insight and will be used to interpret the electronic spectrum. The crystal structure of $[Cr(chxn)_3]Cl_3$ has not been known, but the X-ray structure of *lel*$_3$-$[Cr(chxn)_3](NO_3)_3 \cdot 3H_2O$ at 120 K has been determined.[6] It has been reported that three racemic pairs of isomers are formed in $[Cr(\pm)chxn_3]Cl_3$, with the ratio *lel*$_3$-*lel*$_2$*ob*-*ob*$_2$*lel* = 20 : 4 : 1. The pair of *ob*$_3$-isomers was not detected.[5] We have adapted the positional parame-

Table 2. Peak Positions in the 12 K Sharp-Line Excitation Spectrum of $[Cr(\pm)chxn_3]Cl_3$[a]

$\bar{\nu}$-14881		Assignment	Calcd[b]	Vibronic frequencies	Ground state frequencies[c]
0	vs	R_1		ν_1 119	119
47	vs	R_2		ν_2 164	160
107	vw			ν_3 234	231
123	vw	$R_1+\nu_1$	(119)	ν_4 313	310
166	mw	$R_2+\nu_1$	(116)	ν_5 357	359
211	m	$R_2+\nu_2$	(211)	ν_6 461	464
238	w	$R_1+\nu_3$	(234)	ν_7 484	488
283	vw	$R_2+\nu_3$	(281)		
294	vw				
317	w	$R_1+\nu_4$	(313)		
354	sh	$R_1+\nu_5$	(357)		
364	mw	$R_2+\nu_4$	(361)		
410	mw	$R_2+\nu_5$	(404)		
466	sh	$R_1+\nu_6$	(461)		
482	sh	$R_1+\nu_7$	(484)		
512	s	$R_2+\nu_6$	(508)		
533	s	$R_2+\nu_7$	(531)		
548	ms	$R_1+\nu_3+\nu_4$	(547)		
565	vs	T_1			
591	s	$R_1+\nu_3+\nu_5$	(591)		
607	ms	$R_1+\nu_1+\nu_7$	(603)		
632	m	T_2			
684	m	$T_1+\nu_1$	(684)		
713	m	T_3			
735	mw	$T_1+\nu_2$	(729)		
752	vw	T_2+	(751)		
775	mw	$R_1+\nu_4+\nu_6$	(774)		
793	vw	$T_2+\nu_2$	(793)		
818	vw	$R_1+\nu_5+\nu_6$	(818)		
828	vw	$T_3+\nu_1$	(828)		
844	vw	$R_1+\nu_5+\nu_7$	(841)		
855	w	R_1+859(IR)			
870	vw	$T_3+\nu_2$	(870)		
891	vw	$T_1+2\nu_2$	(893)		
900	w	R_2+859(IR)			
919	vw	$T_1+\nu_5$	(925)		
943	vw	$T_3+\nu_3$	(947)		

[a] Data in cm^{-1}, [b] Values in parentheses represent the calculated frequencies based on the vibrational modes listed, [c] From the luminescence and infrared spectra (Table 1).

ters from the fractional coordinates in the structure of the *lel*$_3$-$[Cr(chxn)_3](NO_3)_3\cdot 3H_2O$. The coordinates were then rotated so as to maximize the projections of the six-coordinated nitrogen atoms on the Cartesian axes centered on the chromium. The resulting Cartesian and spherical coordinates for the nitrate salt are listed in Table 3.

The ligand field analysis was carried out through an optimized fit of experimental to calculated transition energies. The general methods to determine the eigenvalues and eigenfunctions of a d^3 ion in a ligand field from any number

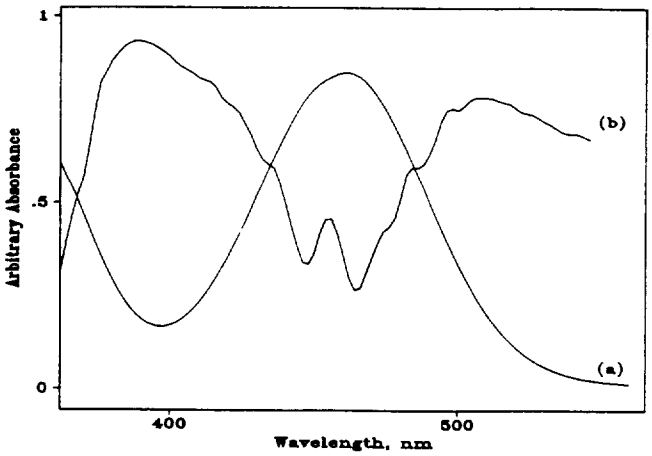

Figure 5. Absorption spectrum of $[Cr(\pm)chxn_3]^{3+}$ in aqueous solution (a) and second derivative (b).

Table 3. Optimized Cartesian and Spherical Polar Coordinates for Ligating Nitrogen Atoms in *lel*$_3$-$[Cr(chxn)_3](NO_3)_3\cdot 3H_2O$[a]

Atom	x	y	z	θ	ϕ
N_1	0.1315	−2.0850	0.1345	86.32	−86.39
N_2	2.0853	0.1337	−0.1305	93.57	3.67
N_3	−0.1337	−0.1314	−2.0839	174.86	−135.50
N_4	−0.1431	−0.1249	2.0635	5.26	−138.89
N_5	0.1245	2.0627	0.1437	86.02	86.55
N_6	−2.0623	0.1437	−0.1238	93.43	176.01

[a] Cartesian coordinates in Å, polar coordinates in degrees.

of atoms in any geometry have been described.[2] The full set of 120 single-term antisymmetrized product wavefunctions was employed as a basis. The Hamiltonian function used in the calculation was

$$H=\sum_{i<j}\frac{e^2}{r_{ij}}+V_{LF}+\zeta\sum_i \boldsymbol{l}_i\cdot\boldsymbol{s}_i+\alpha_T\sum_i \boldsymbol{l}_i^2+2\alpha_T\sum_{i<j}\boldsymbol{l}_i\cdot\boldsymbol{l}_j \quad (1)$$

the terms of which represent, respectively, the interelectronic repulsion, ligand field potential, and spin-orbit coupling, with the last two representing the Trees correction.[15] The π-interactions of a nitrogen with sp^3 hybridization were assumed to be negligible. The parameters varied during the optimization were the interelectronic repulsion parameters B, C and the Trees correction parameter α_T, the spin-orbit coupling parameter ζ, and the AOM parameter $e_{\sigma N}$, which represents the destabilization of a metal d_z^2 orbital pointed directly to a coordinated nitrogen atom. Two separate geometric models were used. In the first model, the one-electron ligand field potential matrix $\langle d_i | V | d_j \rangle$ was generated from the nitrogen positions taken from the crystal structure of the nitrate salt. These five parameters were used to fit eight experimental transition energies: the five $^4A_{2g}\rightarrow\{^2E_g, {}^2T_{1g}\}$ components, identified in Table 3 and the average energies of the transitions to the $^2T_{2g}$, $^4T_{2g}$, and $^4T_{1g}$ states. Eigenvalues were assigned to states within the doublet and quartet manifolds based on an analysis of the corresponding eigenfunctions.[16] The function minimized was

Table 4. Experimental and Calculated Electronic Transition Energies for $[Cr(\pm)chxn_3]Cl_3$[a]

State (O_h)	Exptl	Calcd[b]
^2E_g	14881	14883
	14928	14921
$^2T_{1g}$	15446	15475
	15513	15517
	15594	15565
$^2T_{2g}$ (avg)	22352	22360
$^4T_{2g}$ (avg)	21752	21589
$^4T_{1g}$ (avg)	28303	28289

[a]Data in cm^{-1}. [b]$e_{\sigma N}=7506\pm 9$, $B=703\pm 2$, $C=2953\pm 6$, $\alpha_T=118\pm 2$, $\zeta=275\pm 7$.

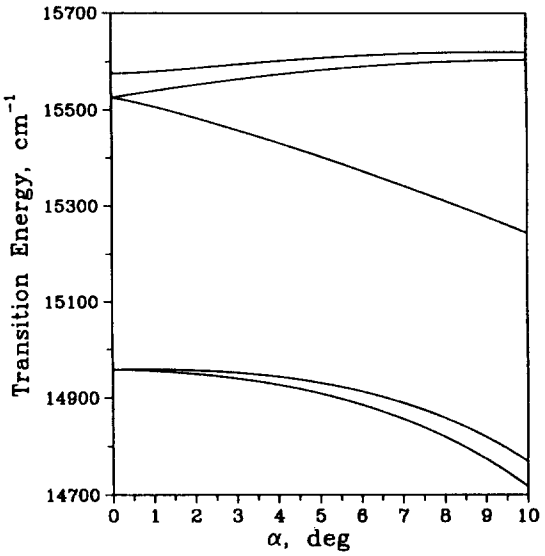

Figure 6. Calculated ^2E_g and $^2T_{1g}$ transition energies for $[Cr(\pm)chxn_3]^{3+}$ as a function of the Cartesian bite angle.

$$f=10^3\ S^2+10^2\sum D^2+10\ T^2+\sum Q^2 \qquad (2)$$

where S in the first term is the ^2E_g splitting and D, T and Q represent the differences between experimental and calculated $\{^2E_g, ^2T_{1g}\}$, $^2T_{2g}$, and $\{^4T_{2g}, ^4T_{1g}\}$ transition energies, respectively. The Powell parallel subspace optimization procedure[17] was used to find the global minimum. The optimization was repeated several times with different sets of starting parameters to verify that the same global minimum was found. The results of the optimization and the parameter set used to generate the best-fit energies are also listed in Table 4. The fit is very good for the sharp-line transitions. The error margins reported for the best-fit parameters in Table 4 are based only on the propagation of the assumed the uncertainties in the observed peak positions.[18] The quartet terms were given a very low weight to reflect the very large uncertainty in their positions.

The sharp-line transition energies, the eight components of the $^4A_{2g}\rightarrow{}^2E_g$, $^2T_{1g}$, and $^2T_{2g}$ transitions, are particularly sensitive to the geometry of the ligand and any other atoms perturbing the metal ion d orbitals. The total angular geometry of an $M(A\text{-}A)_3$ complex with D_3 symmetry can be specified by Cartesian bite (α) and twist (β) angles.[2] The angle β is the amount by which the A-M-A triangle is rotated from the Cartesian plane. We define β as positive when, sighting from the outside towards the central metal, the ligator on the left is displaced upwards and that on the right downwards. The angle α is the angular deviation of a ligand from its Cartesian axis in the Cartesian plane when the triangle is rotated back to that plane. Figures 6 and 7 display the calculated transition energies of the five doublet states of Δ-$[Cr(chxn)_3]^{3+}$ as function of the bite (α) angle and twist (β) angles alone, with the other held to 0°. The input ligand field parameters of the calculation are specified in the bottom of Table 4.

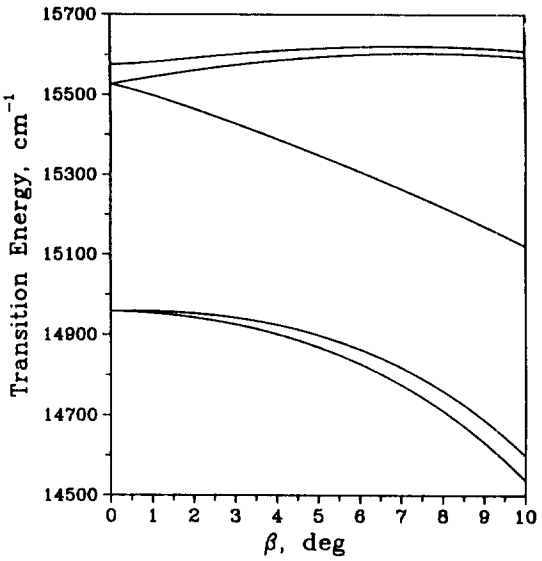

Figure 7. Calculated ^2E_g and $^2T_{1g}$ transition energies for $[Cr(\pm)chxn_3]^{3+}$ as a function of the Cartesian twist angle.

The Cartesian bite and twist distortions have similar effects on the splittings. As they increase, one component of the $^2T_{1g}$ group is expected to move towards the ^2E_g set. It is also apparent that the splittings of the ^2E_g zero-phonon lines increase with the two angles. The observed ^2E_g splitting, 47 cm^{-1} in $[Cr(\pm)chxn_3]Cl_3$, can be comparable to the 4-9 cm^{-1} splitting of the $[Cr(NH_3)_6]^+$ system with near octahedral geometry.[19] According to the X-ray structure determination[6], the Cartesian bite angle in *lel*$_3$-$[Cr(chxn)_3](NO_3)_3\cdot 3H_2O$ is 3.45°. However, it is not reasonable to compared directly the structures of the two salts because contribution[20] from the counterions are possible. We can carefully deduce the Cartesian bite angle of about 3.5° in $[Cr(\pm)chxn_3]Cl_3$ from Figure 4 and the observed ^2E_g splitting. When the optimizing process included the Cartesian bite and twist angles as variable could not be located the global minimum because of the strong interdependence of the two angles. The relative d-orbital ordering from the calculations is xy(1.2 cm^{-1})<xz (547 cm^{-1})<yz(551 cm^{-1})<x^2-y^2(21,969 cm^{-1})<z^2(21,973 cm^{-1}). The value, 7,506 cm^{-1} for the $e_{\sigma N}$ parameter obtained from the complete ligand field analysis is a little smaller than the 7,721 cm^{-1} reported for $[Cr(tacn)_2]Cl_3$,[21] but it does not differ much from that for $[Cr(en)_3]^{3+}$ complex.[22] This indicates that the presence of the fused cyclohexane ring has little affect on the metal-ligand bonding properties. It is safe

to conclude that the nitrogen atoms of chxn is strong σ-donor toward chromium(III). The value of $e_{\sigma N}$ is also located within the normal range[23] for metal-ligand bonding properties of chromium(III) complexes. The complete ligand field parameters reported here may be transferable to other complexes as a basis for schematic analysis of this type of saturated hexaamine system.

Acknowledgements. The author wishes to thank Professor Patrick E. Hoggard for fruitful cooperation and Dr. Thomas Schönherr for measurements of far infrared spectra. Financial support of the Korea Science and Engineering Foundation is also gratefully acknowledged.

References

1. (a) This is part 14 of the series *Electronic Structure and Chemical Reactivity of Transition Metal Complexes*; (b) The preceding publication in this series is Ref. 1(d); (c) Abbreviations used: chxn=*trans*-1,2-cyclohexanediamine, en=1,2-ethanediamine, tacn=1,4,7-triazacyclononane; (d) Choi, J-H.; Oh, I-G. *Bull. Basic Sci. Andong Univ.* **1993**, *4*, 15.
2. Hoggard, P. E. *Coord. Chem. Rev.* **1986**, *70*, 85; (b) Hoggard, P. E. *Curr. Top. Chem.* **1993**, in press.
3. (a) Wilson, R. B.; Solomon, E. I. *Inorg. Chem.* **1978**, *17*, 1729; (b) Flint, C. D.; Matthews, A. P. *J. Chem. Soc. Faraday Trans. II*, **1976**, *72*, 579; (c) Choi, J-H. *Bull. Korean Chem. Soc.* **1993**, *14*, 118; (d) Choi, J-H.; Oh, I-G. *Bull. Korean Chem. Soc.* **1993**, *14*, 348.
4. Wasgestian, F.; Gowin, E. *Inorg. Chim. Acta* **1986**, *L27*, 120.
5. Harnung, S. E.; Laier, T. *Acta Chem. Scand.* **1978**, *32A*, 41.
6. Morooka, M.; Ohba, S.; Miyamae, H. *Acta Cryst.* **1992**, *B48*, 667.
7. (a) Iida, M.; Iwaki, M.; Matsuno, Y.; Yokoyama, H. *Bull. Chem. Soc. Jpn.* **1990**, *63*, 993; (b) Iida, M.; Yokoyama, H. *Bull. Chem. Soc. Jpn.* **1991**, *64*, 128.
8. Kaizaki, S.; Ito, M.; Nishimura, N.; Matsushita, Y. *Inorg. Chem.* **1985**, *24*, 2080.
9. Pederson, E. *Acta Chem. Scand.* **1970**, *24*, 3362.
10. Lever, A. B. P. *Inorganic Electronic Spectroscopy*, 2nd ed.; Elsevier: Amsterdam, **1984**.
11. Sonar, M. H.; Murty, A. S. R. *J. Inorg. Nucl. Chem.* **1977**, *39*, 2155.
12. Choi, J-H.; Hoggard, P. E. *Polyhedron*, **1992**, *11*, 2399.
13. Nakagawa, I.; Shimanouchi, T. *Spectrochim. Acta* **1966**, *22*, 759.
14. Geiser, U.; Güdel, H. U. *Inorg. Chem.* **1981**, *20*, 3013.
15. Trees, R. E. *Phys. Rev.* **1951**, *83*, 756.
16. Hoggard, P. E. *Inorg. Chem.* **1991**, *30*, 4644.
17. (a) Powell, M. J. D. *Computer J.* **1964**, *7*, 155; (b) Kuester, J. L.; Mize, J. H. *Optimization Techniques with Fortran*; McGraw-Hill: New York, 1973.
18. Clifford, A. A. *Multivariate Error Analysis* Wiley-Halsted: New York, 1973.
19. Urushiyama, A.; Schönherr, T.; Schmidtke, H-H. *Ber. Bunsenges. Phys. Chem.* **1986**, *90*, 1188.
20. Lee, K-W.; Hoggard, P. E. *Inorg. Chem.* **1988**, *27*, 2335.
21. Lee, K-W.; Hoggard, P. E. *Transition Met. Chem.* **1991**, *16*, 377.
22. Hoggard, P. E. *Inorg. Chem.* **1988**, *27*, 3477.
23. Lever, A. B. P. *Coord. Chem. Rev.* **1982**, *43*, 63.

Preparation and Structure of $Re(\equiv NC_6H_5)(CO)(PPh_3)Cl_3$

Young-Woong Kim, June-Ho Jung, and Soon W. Lee*

Department of Chemistry, Sung Kyun Kwan University, Suwon 440-746

Received September 23, 1993

By treating *mer, trans*-$Re(\equiv NC_6H_5)(PPh_3)_2Cl_3$, I, with 5 atm of CO at room temperature for 52 h, *fac*-$Re(\equiv NC_6H_5)(CO)(PPh_3)Cl_3$, II, was obtained as dark green precipitates in 81% yield. The crystal structure of II was determined through X-ray diffraction. II crystallizes in the monoclinic system, space group $P2_1/n$ with cell parameters $a=9.740$ (2) Å, $b=16.210$ (5) Å, $c=16.192$ (6) Å, $\beta=97.50$ (2)°, and $Z=4$. Least-squares refinement of the structure led to a $R(R_w)$ factor of 0.030 (0.036) for 2878 unique reflections of $I>3\sigma(I)$ and for 241 variables. In comparison to the starting material I, the bond distance of Re-N became longer from 1.726 (6) to 1.736 (5) Å and the bond angle of Re-N-C(Ph) became smaller from 172.6 (6) to 167.0 (2)°, indicating that the Re-N bond in II is weakened and has a less triple-bond character than that in I.

Introduction

Since the first nitrene complexes, $OsO_3(NR)$, were reported in 1959, transition-metal nitrene (or imido) complexes have received continuous interest[1]. They are presumed to be involved in catalytic processes in such as propylene ammoxidation[2], nitrile reduction[3], and very recently hydrodenitrogenation catalysis[4]. Very recently, Bergman and his workers reported an insertion of CO into an Ir≡N bond in $Cp^*Ir(\equiv N^tBu)(Cp^*=C_5(CH_3)_5)$, which is the first carbonylation of a terminal imido ligand to give an isocyanate complex[5]. The results of above studies prompted us to investigate the possibility of insertion